# The Effects of Silver Content and Solidification Profile on the Anand Constitutive Model for SAC Lead Free Solders

Munshi M. Basit, Mohammad Motalab, Jordan C. Roberts, Jeffrey C. Suhling, Pradeep Lall
Center for Advanced Vehicle and Extreme Environment Electronics, and
Department of Mechanical Engineering
Auburn University
Auburn, AL 36849
Phone: +1-334-844-3332
FAX: +1-334-844-3124
E-Mail: jsuhling@eng.auburn.edu

## ABSTRACT

In the electronic packaging industry, it is important to be able to make accurate predictions of board level solder joint reliability during thermal cycling exposures. The Anand viscoelastic constitutive model is often used to represent the material behavior of the solder in finite element simulations. This model is defined using nine material parameters, and the reliability prediction results are often highly sensitive to the Anand parameters. In this work, an investigation on the Anand constitutive model and its application to SAC solders of various Ag contents (i.e. SACN05, with N = 1, 2, 3, 4) has been performed. For each alloy, both water quenched (WQ) and reflowed (RF) solidification profiles were utilized to establish two unique specimen microstructures, and the same reflow profile was used for all four of the SAC alloys so that the results could be compared and the effects of Ag content could be studied systematically.

The nine Anand parameters were determined for each unique solder alloy and microstructure from a set of stress-strain tests performed at several strain rates and temperatures. Testing conditions included strain rates of 0.001, 0.0001, and 0.00001 ($sec^{-1}$), and temperatures of 25, 50, 75, 100, and 125 C. The Anand parameters were calculated from each set of stress-strain data using an established procedure that is described in detail in the paper. Using the calculated results for the various SAC alloys and microstructures, a set of empirical models have been established to describe the effects of SAC alloy Ag content on the Anand model parameters.

As expected, the mechanical properties (modulus and strength) increase with the percentage of Ag content, and these changes strongly affect the Anand parameters. The sensitivity of the mechanical properties and Anand parameters to silver content is higher at lower silver percentages (1-2%). Also, the observed mechanical properties of water quenched samples were better (higher in magnitude) than the corresponding mechanical properties of the reflowed samples. Although the differences in elastic modulus between the water quenched and reflowed samples are small, significant differences are present for the yield and ultimate tensile stresses of all four SAC alloys. After deriving the Anand parameters for each alloy, the stress-strain curves have been calculated for various conditions, and excellent agreement was found between the predicted results and experimental stress-strain curves.

**KEY WORDS:** Lead Free Solder, Ag Content, Solidification Profile, Anand Model, Constitutive Relations

## NOMENCLATURE

| | |
|---|---|
| $\sigma$ | Uniaxial Stress |
| $\varepsilon$ | Uniaxial Strain |
| $\sigma_u$ | Ultimate Tensile Strength (UTS) |
| $\sigma_Y$ | Yield Stress |
| $\dot{\varepsilon}_p$ | Inelastic (Plastic) Strain Rate |
| T | Temperature |
| s | Internal Variable |
| $\xi$ | Multiplier of Stress |
| A | Pre-Exponential Factor |
| Q | Activation Energy |
| R | Universal Gas Constant |
| $h_o$ | Hardening Constant |
| $s_o$ | Internal Variable Initial Value |
| s* | Saturation Value of Internal Variable |
| $\hat{s}$ | Coefficient for Deformation Saturation Value |
| m | Strain Rate Sensitivity of Stress |
| n | Strain Rate Sensitivity of Saturation Process |
| a | Strain Rate Sensitivity of the Hardening Process |
| WQ | Water Quenched |
| RF | Reflowed |

## INTRODUCTION

The electronic packaging industry has transitioned to Pb-free solders due to environmental concerns. Among the diversity of Pb-free solders, the Sn-Ag-Cu (SAC) alloys have become the most popular and are often considered to be the standard lead-free alloys. NEMI (National Electronics Manufacturing Initiative) recommended to replace Sn-Pb solders by eutectic Sn-Ag-Cu solder in reflow processing and eutectic Sn-Cu solder in wave soldering [1]. Depending on the percentage of silver (Ag), there are several types of SAC alloys available in the market. Solder joint fatigue life under thermal cycling has been shown to increase with increasing Ag content in the SAC solders joints, due to improved mechanical properties and increased fatigue resistance [2]. However, the drop performance of electronic assemblies with SAC Pb-free solder joints is often reduced when increasing the Ag content in the SAC solder [3]. Low silver content solders are increasingly used in electronic assembly for handheld electronic products to improve the drop performance

of the solder joints and to lower costs. Hence, there are trade-offs based on the silver content, and no one SAC alloy is typically suitable for all applications.

Ma, et al. [4] have reviewed the literature on the mechanical behavior of lead free solders. Several researchers have studied the effect of Ag content on the mechanical, thermal, fatigue performance of SAC alloys. For example, Che, et al. [5] have measured stress-strain curves for various SAC alloys at different strain rates, while Zhu, et al. [6] have measured the mechanical properties of SAC305 at different strain rates and temperatures.

The mechanical properties of a lead free solder are strongly influenced by its microstructure, which is controlled by its thermal history including solidification rate and thermal aging after solidification. Due to aging phenomena, the microstructure, mechanical response, and failure behavior of lead free solder joints in electronic assemblies are constantly evolving when exposed to isothermal aging and/or thermal cycling environments. Such aging effects are greatly exacerbated at higher temperatures typical of thermal cycling qualification tests. However, significant changes occur even with aging at room temperature.

The effects of aging on the constitutive and failure behavior of lead free solder have been extensively investigated by the authors [7-20]. In initial work, room temperature (25 C) and elevated temperature (50, 75, 100, and 125 C) aging were shown to severely degrade the mechanical properties and creep behavior of several SAC alloys including SAC105, SAC205, SAC305, and SAC405 [7-12]. The measured stress-strain data demonstrated large reductions in stiffness, yield stress, ultimate strength, and strain to failure (up to 50%) during the first 6 months after reflow solidification. After approximately 10-20 days of aging, the lead free solder joint material properties were observed to degrade at a slow but constant rate. In addition, even more dramatic evolution was observed in the creep response of aged solders, where up to 10,000X increases in the secondary creep rates were observed for aging up to 6 months. The aged solder materials were also found to enter the tertiary creep range (imminent failure) at much lower strain levels than virgin solders (non-aged, tested immediately after reflow solidification). All of the degradations in behavior due to aging effects were found to be exacerbated in SAC solders with lower silver content. Zhang, et al. have explored aging effects in mixed solder alloys (SAC and Sn-Pb) [11], while Cai and coworkers [12] have demonstrated that such aging effects can be reduced in lower Ag content alloys through the use of dopants (i.e., SAC-X).

Mustafa, et al. have studied the aging-induced changes occurring in the cyclic stress-strain behavior of lead free SAC solders for both tension/compression [13] and shear [14] loadings. The effects of several parameters were examined including aging time, temperature, strain/stress limits, and solder alloy composition. In addition, the evolution of the solder hysteresis loops with aging were characterized and empirically modeled. Similar to solder stress-strain and creep behavior, there was a strong influence of aging on the hysteresis loop size (and thus the rate of damage accumulation) in the solder specimens. Also, degradations were higher for the low Ag content alloys.

Zhang, et al. [15-16] have shown that prior aging causes large reductions in the reliability of BGA test assemblies subjected thermal cycling accelerated life testing. Motalab, et al. [17-18] have included aging effects in the Anand constitutive model and energy density based failure criterion for SAC solders, and then used these theories with finite element analyses to predict the thermal cycling life of aged BGA assemblies. Good correlations were achieved with the measured lifetimes from references [15-16]. Finally, Hasnine, et al. [19] have used nanoindentation to study the evolution of mechanical properties and creep rates in BGA solder joints subjected to aging, while Lall and coworkers [20] have investigated changes in the high strain rate behavior of SAC solders subjected to aging.

The Anand viscoelastic constitutive model [21] is often used to represent the material behavior of the lead free solders in finite element simulations. This model is defined using nine material parameters, and the reliability prediction results are often highly sensitive to the values of the Anand parameters. There are several publications listing values of Anand parameters for particular solder alloys. For example, Anand parameters for alloys such as Sn-3.5Ag, SAC105, SAC305, and SAC387 have been documented [17-18, 22-25]. However, there has been no systematic study by a single group on how the Anand parameters for SAC alloys vary with the percentage of Ag in the alloy. As discussed above, the silver content of a SAC alloy has been shown to be critical in optimizing thermal cycling and drop reliability of lead free electronics.

In this work, we have performed an investigation on the Anand constitutive model and its application to SAC solders of various Ag contents (i.e. SACN05, with N = 1, 2, 3, 4). For each alloy, both water quenched (WQ) and reflowed (RF) solidification profiles were utilized to establish two unique specimen microstructures, and the same reflow profile was used for all four of the SAC alloys so that the results could be compared and the effects of Ag content could be studied systematically.

The nine Anand parameters were determined for each unique solder alloy and microstructure from a set of stress-strain tests performed at several strain rates and temperatures. Testing conditions included strain rates of 0.001, 0.0001, and 0.00001 ($sec^{-1}$), and temperatures of 25, 50, 75, 100, and 125 C. The Anand parameters were calculated from each set of stress-strain data using an established procedure that is described in detail in the paper. Using the calculated results for the various SAC alloys and microstructures, a set of empirical models have been established to describe the effects of SAC alloy Ag content on the Anand model parameters. After deriving the Anand parameters for each alloy, the stress-strain curves have been calculated for various conditions, and excellent agreement was found between the predicted results and experimental stress-strain curves.

## ANAND VISCOPLASTIC CONSTITUTIVE MODEL

### Introduction

The viscoplastic constitutive equations proposed by Anand [21] have become popular for rate-dependent deformation of metals at high temperatures. They were initially developed for structural metals such as aluminum, but have been adopted for microelectronic solders (Sn-Pb and lead free) for homologous temperatures in excess of $0.5T_m$.

The so-called Anand model has been widely applied for the solder stress-strain relations in finite element simulations of electronic packages, where solders undergo small elastic deformations and large viscoplastic deformations. For example, Che, et al. [26] have considered multiple constitutive theories, and then demonstrated that the Anand equations were well matched with predictions of lead free solder fatigue life. In addition, Pei and coworkers [27] have calculated the nine parameters of the Anand model by conducting tensile testing of Sn3.5Ag and Sn3.8Ag0.7Cu lead free solders at several temperatures and strain rates.

Mysore, et al. [28] have found the Anand material parameters for SAC305 (Sn3.0Ag0.5Cu) lead free solder alloy by performing double lap shear tests. They suggested that the Anand parameters for solder joint samples are significantly different than those measured by testing of bulk solder specimens. In addition, Motalab, et al. [29] have evaluated the Anand parameters for SAC305 solder using two approaches, including stress-strain testing and creep testing. Bai and coworkers [30] suggested a modified approach for SAC305 (Sn3.0Ag0.5Cu) lead free solder where strain rate and temperature dependent values were included for Anand model parameter $h_o$. The Anand model constants for SAC105 (Snl.0Ag0.5Cu) lead free solder have been reported for Amagai, et al. [22] and Kim, et al. [31].

### Review of Anand Model Equations (1D)

The authors [17-18, 29] have previously reviewed the general equations of the Anand constitutive model for one-dimensional (uniaxial) stress states. The theoretical approach is based on a scalar internal variable s, which represents the material resistance to plastic flow. The model includes three equations: (1) stress equation, (2) flow equation, and (3) evolution equation. These expressions unify the rate-independent plastic behavior and creep behavior of the material. The Anand model does not contain an explicit yield condition or a loading/unloading criterion.

The stress equation is expressed as

$$\sigma = cs;\ c < 1 \tag{1}$$

where s is the scalar internal valuable. Quantity c is a function of the temperature and strain rate, and is given by

$$c = c(\dot{\varepsilon}_p, T) = \frac{1}{\xi}\sinh^{-1}\left\{\left[\frac{\dot{\varepsilon}_p}{A} e^{\left(\frac{Q}{RT}\right)}\right]^m\right\} \tag{2}$$

where $\dot{\varepsilon}_p$ is the plastic strain rate, A is the pre-exponential factor, $\xi$ is the multiplier of stress, m is the strain rate sensitivity, Q is the activation energy, R is the universal gas constant, and T is the absolute temperature. By substitution of eq. (2) into eq (1), the reformatted stress equation becomes:

$$\sigma = \frac{s}{\xi}\sinh^{-1}\left\{\left[\frac{\dot{\varepsilon}_p}{A} e^{\left(\frac{Q}{RT}\right)}\right]^m\right\} \tag{3}$$

The Anand model flow equation is found by solving for the strain rate in eq.(3):

$$\dot{\varepsilon}_p = A e^{-\left(\frac{Q}{RT}\right)}\left[\sinh\left(\xi\frac{\sigma}{s}\right)\right]^{\frac{1}{m}} \tag{4}$$

The evolution equation describes the variation of internal variable s with time. In its differential form, it can be expressed as:

$$\dot{s} = h(\sigma, s, T)\dot{\varepsilon}_p$$
$$\dot{s} = \left[h_o\left(1-\frac{s}{s^*}\right)^a \operatorname{sign}\left(1-\frac{s}{s^*}\right)\right]\dot{\varepsilon}_p;\quad a > 1 \tag{5}$$

The term $h(\sigma, s, T)$ in eq. (5) is associated with dynamic hardening and recovery, and its initial value is the hardening constant $h(0) = h_o$. Parameter a is the strain rate sensitivity of the hardening process, and parameter s* is the saturation value of the deformation resistance given by

$$s^* = \hat{s}\left[\frac{\dot{\varepsilon}_p}{A} e^{\left(\frac{Q}{RT}\right)}\right]^n \tag{6}$$

where $\hat{s}$ is a coefficient, and n is the strain rate sensitivity. Equation (5) can be expressed as

$$ds = h_o\left(1-\frac{s}{s^*}\right)^a d\varepsilon_p \tag{7}$$

for $s < s^*$, and then integrated resulting in an evolution expression for the internal variable s:

$$s = s^* - \left[\left(s^* - s_o\right)^{(1-a)} + (a-1)\left\{(h_o)\left(s^*\right)^{-a}\right\}\varepsilon_p\right]^{\frac{1}{1-a}} \tag{8}$$

where the initial value is $s(0) = s_o$ at time $t = 0$. Combining eq. (6) and eq. (8) results in an evolution equation for the internal variable s in terms of the plastic strain and plastic strain rate:

$$s = \hat{s}\left[\frac{\dot{\varepsilon}_p}{A}e^{\left(\frac{Q}{RT}\right)}\right]^n - \left[\begin{array}{l}\left(\hat{s}\left[\frac{\dot{\varepsilon}_p}{A}e^{\left(\frac{Q}{RT}\right)}\right]^n - s_o\right)^{(1-a)} + \\ (a-1)\left\{(h_o)\left(\hat{s}\left[\frac{\dot{\varepsilon}_p}{A}e^{\left(\frac{Q}{RT}\right)}\right]^n\right)^{-a}\right\}\varepsilon_p\end{array}\right]^{\frac{1}{1-a}} \quad (9)$$

or

$$s = s(\dot{\varepsilon}_p, \varepsilon_p) \quad (10)$$

The final versions of the Anand model equations are the stress equation in eq. (3), the flow equation in eq. (4), and the integrated evolution equation in eq. (9). These expressions include 9 material parameters: A, $\xi$, Q/R, m in eqs. (3, 4); and constants $h_o$, a, $s_o$, $\hat{s}$, and n in eq. (9).

**Uniaxial Stress-Strain Theoretical Response**

Equations (3) and (9) can be combined to give an expression for the uniaxial stress-strain law (post yield) predicted by the Anand model:

$$\sigma = \frac{1}{\xi}\sinh^{-1}\left\{\left[\frac{\dot{\varepsilon}_p}{A}e^{\left(\frac{Q}{RT}\right)}\right]^m\right\}\left(\begin{array}{l}\hat{s}\left[\frac{\dot{\varepsilon}_p}{A}e^{\left(\frac{Q}{RT}\right)}\right]^n - \\ \left[\begin{array}{l}\left(\hat{s}\left[\frac{\dot{\varepsilon}_p}{A}e^{\left(\frac{Q}{RT}\right)}\right]^n - s_o\right)^{(1-a)} + \\ (a-1)\left\{(h_o)\left(\hat{s}\left[\frac{\dot{\varepsilon}_p}{A}e^{\left(\frac{Q}{RT}\right)}\right]^n\right)^{-a}\right\}\varepsilon_p\end{array}\right]^{\frac{1}{1-a}}\end{array}\right)$$

$$\sigma = \sigma(\dot{\varepsilon}_p, \varepsilon_p) \quad (11)$$

For a uniaxial tensile test performed at fixed (constant) strain rate $\dot{\varepsilon}_p$ and constant temperature T, this equation represents nonlinear stress-strain behavior in the form of a power law type function after yielding:

$$\sigma = \sigma(\varepsilon_p) \quad (12)$$

The yield stress ($\sigma_Y$) and the Ultimate Tensile Strength (UTS = maximum or saturation stress) can be obtained from eq. (11) by taking the limits for small and large plastic strains. The yield stress is given by the limit as $\varepsilon_p$ goes to 0:

$$\sigma_Y = \sigma\big|_{\varepsilon_p \to 0} = cs_0 = \frac{1}{\xi}\sinh^{-1}\left\{\left[\frac{\dot{\varepsilon}_p}{A}e^{\left(\frac{Q}{RT}\right)}\right]^m\right\} s_0 = c\,s_0 \equiv \sigma_0 \quad (13)$$

while the UTS is given by the limit as $\varepsilon_p$ goes to $\infty$:

$$UTS = \sigma\big|_{\varepsilon_p \to \infty} = \frac{\hat{s}}{\xi}\left[\frac{\dot{\varepsilon}_p}{A}e^{\left(\frac{Q}{RT}\right)}\right]^n \sinh^{-1}\left\{\left[\frac{\dot{\varepsilon}_p}{A}e^{\left(\frac{Q}{RT}\right)}\right]^m\right\} \equiv \sigma^* \quad (14)$$

By substituting eq. (14) into eq. (11), the stress-strain power law relation after yielding can be expressed as:

$$\sigma = \sigma^* - \left[(\sigma^* - c\,s_0)^{(1-a)} + (a-1)\left\{(ch_0)(\sigma^*)^{-a}\right\}\varepsilon_p\right]^{1/(1-a)} \quad (15)$$

**Procedure for Determining the Anand Model Parameters from Uniaxial Stress Strain Data**

Anand [21] suggested using stress-strain data measured over a wide range of temperatures and strain rates to determine the 9 parameters (A, $\xi$, Q/R, m, $h_o$, a, $s_o$, $\hat{s}$, and n) in the viscoelastic constitutive relations presented above. In our previous studies [17-18, 29], we have outlined a procedure for performing this task. Values of the saturation stress ($\sigma^*$ = UTS) can be extracted from the peak stress values on the stress-strain curves for several temperatures and strain rates. Also, stress vs. plastic strain data ($\sigma$ vs. $\varepsilon_p$) can extracted from the recorded stress-strain curves ($\sigma, \varepsilon$) at the various temperatures and strain rates. The conversion of total strain to plastic strain for each data set is performed using:

$$\varepsilon_p = \varepsilon - \frac{\sigma}{E} \quad (16)$$

where E is the initial elastic modulus. The sequential procedure for calculating the Anand model parameters consists of:

1. The six Anand parameters $\hat{s}$, $\xi$, A, Q/R, n and m are determined using a nonlinear least-squares regression fit of eq. (14) to the recorded saturation stress (UTS) vs. temperature and strain rate data.
2. The remaining three Anand parameters ($s_o$, $h_o$, and a) are found using nonlinear regression fits of eq. (15) to the recorded stress vs. plastic strain data at several temperatures and strain rates.

**EXPERIMENTAL PROCEDURE**

**Test Matrix**

The solder alloy test matrix is shown in Table 1. The SAC solder alloys investigated in this work include 98.5Sn1.0Ag0.5Cu (SAC105), 97.5Sn2.0Ag0.5Cu (SAC205), 96.5Sn3.0Ag0.5Cu (SAC305), and 95.5Sn4.0Ag0.5Cu (SAC405). Stress-strain tests on the SACN05 (N = 1, 2, 3, 4) lead free solder samples were performed for samples prepared by both water quenched and reflow cooling profiles. For each SACN05 alloy and microstructure (cooling profile), stress-strain experiments were performed at five temperatures (T = 25, 50, 75, 100, and 125 C), and three strain rates ($\dot{\varepsilon}$ = .001, .0001, and .00001 $sec^{-1}$) as indicated in Table 2. Using the measured stress-strain data and calculation procedure

presented above, the nine Anand model parameters have been determined for the SACN05 alloys in Table 1.

Table 1 - SAC Solder Test Matrix

| | SACN05 | | | |
|---|---|---|---|---|
| | SAC105 | SAC205 | SAC305 | SAC405 |
| RF | √ | √ | √ | In Progress |
| WQ | √ | √ | √ | √ |

Table 2 - Text Matrix for a Particular SACN05 Alloy

| Temp. (C) | Reflow (RF) | | | Water Quenched (WQ) | | |
|---|---|---|---|---|---|---|
| | $10^{-3}$/s | $10^{-4}$/s | $10^{-5}$/s | $10^{-3}$/s | $10^{-4}$/s | $10^{-5}$/s |
| 25 | √ | √ | √ | √ | √ | √ |
| 50 | √ | √ | √ | √ | √ | √ |
| 75 | √ | √ | √ | √ | √ | √ |
| 100 | √ | √ | √ | √ | √ | √ |
| 125 | √ | √ | √ | √ | √ | √ |

**Uniaxial Test Sample Preparation**

Solder material characterization is typically performed by uniaxial loading of machined or mold cast samples, or by shear loading of joint samples. In the current study, a vacuum suction process was utilized to form solder uniaxial test specimens with controlled microstructure in high precision rectangular cross-section glass tubes [7-14]. Initially, bulk solder material is melted in a quartz crucible using circular heating elements (see Figure 1). The heater in the melting process is excited using a digital controller, which uses feedback from a thermocouple attached on the crucible. The solder is drawn into the glass tube by inserting one end into the molten solder in the crucible, and then applying suction to the other end using a rubber tube connected to a vacuum source. The amount of solder drawn into the tube is controlled using a regulator on the vacuum line. After the desired amount of solder fills the tube, it is solidified by quenching in a room temperature water bath.

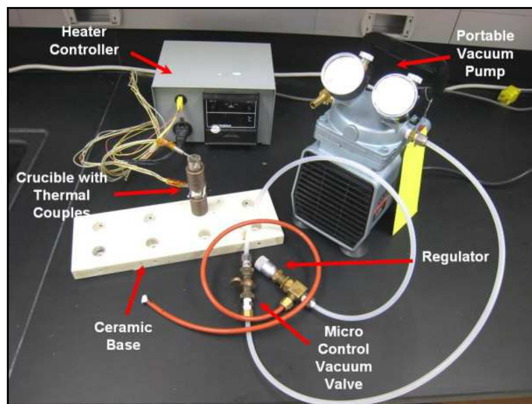


Figure 1 - Sample Preparation System

Tensile specimens were prepared using both water quenched (WQ) and reflowed (RF) solidification profiles. The temperature vs. time variations for the two profiles are shown in Figure 2. As discussed above, all of the glass tube solder samples were first water quenched. This extremely quick cooling returned the molten solder to room temperature within 10 sec, and yielded very fine microstructure test samples. After quenching, the specimens to be reflowed were subsequently sent through a reflow oven to re-melt the solder in the tubes. In this work, we used a nine zone Heller 1800EXL oven, which allowed a great flexibility in tailoring the temperature profile. The lead free profile in this work (Figure 2b) was chosen to match one that is typical for BGA solder joints. A radio-frequency KIC temperature profiling system was used to monitor the solder temperature and control the reflow process using thermocouples attached to the glass tubes.

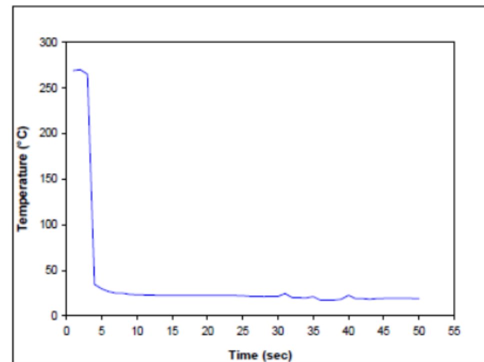


(a) Water Quenched

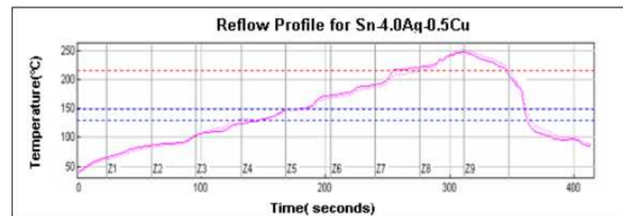


(b) Reflowed

Figure 2 - Temperature Profiles for SAC Solder

Figure 3 shows typical solder-filled glass tube assemblies and a final extracted specimen. For some alloys, the solidified solder samples were easily pulled from the tubes due to the differential expansions that occur in the glass tube (low CTE) and solder (high CTE) during cooling. Specimens formed from the lower silver content SAC alloys typically required a more destructive removal process (breaking the glass). The tubes in this work had a length of 120 mm, and a cross-sectional area of 3.0 x 0.5 mm. A thickness of 0.5 mm was chosen since it matches the height of typical BGA solder joints. The nominal dimensions of the final test samples were 80 x 3 x 0.5 mm. The specimens were stored in a low temperature freezer after the water quenched/reflow process to minimize any aging effects.

The solder microstructure has been verified to be consistent throughout each specimen volume, and from specimen to specimen by cross-sectioning. A micro-focus x-ray system was used to inspect the samples for the presence of

flaws (e.g. notches and external indentations) and/or internal voids (non-visible). Specimens with no flaws and voids were generated using proper experimental techniques, and Figure 4 illustrates x-rays scans for good and poor specimens.

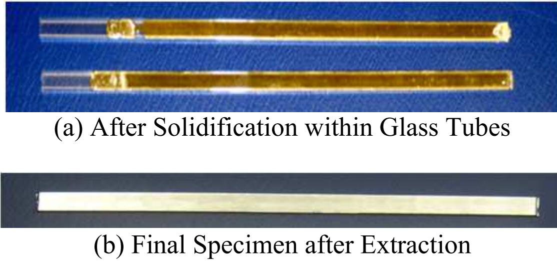

(a) After Solidification within Glass Tubes

(b) Final Specimen after Extraction

Figure 3 - Solder Uniaxial Test Specimens

Figure 4 - X-Ray Scans of Solder Test Specimens (Good and Bad Samples)

**Mechanical Testing System**

Figure 5 shows the tension/torsion thermo-mechanical test system (Wisdom Technology MT-200) used to perform the stress-strain tests in this study. This instrument is optimized for loading small specimens such as thin films, solder joints, gold wire, fibers, etc. It provides an axial displacement resolution of 0.1 micron. Samples can be tested over a temperature range of -185 to +300 C using supplemental environmental chambers added to the system.

Figure 5 - Mechanical Test System with Solder Sample

Forces and displacements were measured in the uniaxial tests, and the axial stress and axial strain were calculated using

$$\sigma = \frac{F}{A} \qquad \varepsilon = \frac{\Delta L}{L} = \frac{\delta}{L} \tag{17}$$

where F is the measured uniaxial force, $\delta$ is the measured crosshead displacement, $\sigma$ is the uniaxial stress, $\varepsilon$ is the uniaxial strain, A is the original cross-sectional area, and L = 60 mm is the chosen specimen gage length (initial length between the grips).

**Typical Test Data**

Figure 6 illustrates a typical SAC solder tensile stress strain curve. The standard material properties are labelled on the graph including the effective elastic modulus E (initial slope of the stress-strain curve). This effective modulus is rate dependent since solder behavior is viscoplastic. The value of the effective modulus will become the true elastic modulus as the testing speed is increased to the limit of infinite strain rate. The yield stress $\sigma_Y$ (YS) is defined using the typical definition of the stress level that results in a permanent strain of $\varepsilon = .002$ = .2% upon unloading. The maximum (saturation) stress on the stress-strain curve is the ultimate tensile strength $\sigma_u$ (UTS).

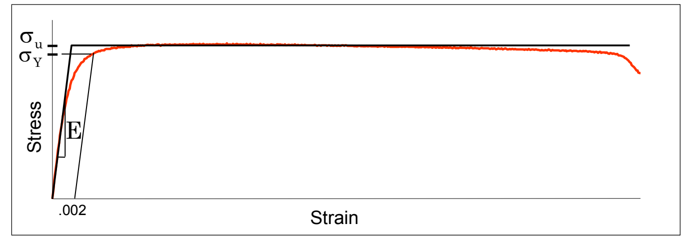


Figure 6 - SAC Stress-Strain Curve and Material Properties

**Stress-Strain Data Processing**

Figure 7 illustrates a typical set of 10 solder stress strain curves measured for the same alloy under similar environmental and aging conditions. In this work, a four parameter hyperbolic tangent empirical model

$$\sigma = C_1 \tanh(C_2\varepsilon) + C_3 \tanh(C_4\varepsilon) \tag{18}$$

has been used to represent the "average" stress-strain curve through a set of experimental data (red curve in Figure 7). Material constants $C_1$, $C_2$, $C_3$, $C_4$ are determined through regression fitting of the model to experimental data. The effective elastic modulus E at zero strain is calculated from the model constants using

$$E = \sigma'(0) = C_1C_2 + C_3C_4 \tag{19}$$

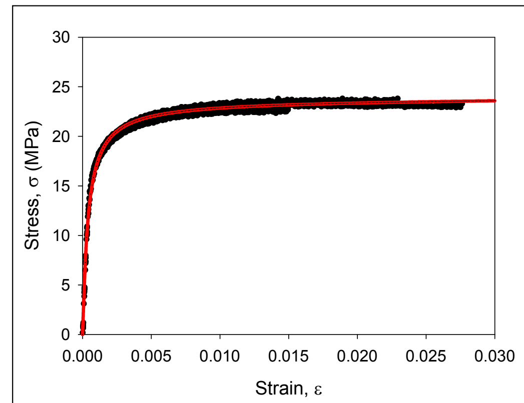


Figure 7 - Empirical Model Fit to Solder Stress-Strain Curves

## RESULTS FOR SACN05

### Effects of Ag Content and Solidification Profile on the Stress-Strain Curves and Material Properties

The recorded stress-strain curves for the four SACN05 alloys and a strain rate of 0.001 $sec^{-1}$ are shown in Figures 8 and 9 for the water quenched and reflowed cooling profiles, respectively. Each curve in these plots is an "average" stress-strain curve representing the fit of the empirical model in eq. (18) to the 10 recorded stress-strain curves for a given SAC alloy, strain rate, and temperature. The five colored curves in each graph are the stress-strain results for temperatures of T = 25 (black), 50 (blue), 75 (green), 100 (brown), and 125 C (red). As expected, the data for the various SAC alloys all demonstrate a steady decline in the effective elastic modulus, yield stress (YS), and ultimate tensile strength (UTS) with temperature. For example, Figure 10 illustrates the variation of mechanical properties (E, YS, UTS) with temperature for the water quenched SACN05 alloys and a strain rate of 0.001 $sec^{-1}$. The observed degradations have an approximately linear variation with temperature. In addition, the material properties increase dramatically with the percentage of Ag present in the SAC alloy.

Analogous results were found for the material properties of the reflowed alloys at the strain rate of 0.001 $sec^{-1}$. For example, a comparison of the UTS values for the four SACN05 alloys in bar graph form are shown in Figure 11 for the water quenched and reflowed microstructures. From these plots, it is clear that the largest percentage changes in strength occur between SAC105 and SAC205. For example, the UTS (WQ) values at T = 25 C for SAC105, SAC205, SAC305, and SAC405 are 47.2 MPa, 65.0 MPa, 74.1 MPa, and 81.7 MPa, respectively. In this case, the strength of SAC205 is 38% higher than that for SAC105, while SAC305 and SAC405 show additional increases of 14% and 10.2%, respectively. The Ag content affects the size and density of the $Ag_3Sn$ intermetallic compound (IMC) precipitates. Increasing the Ag content of the solder causes it to exhibit higher strength and fatigue resistance because of precipitate strengthening [32].

The corresponding experimental stress-strain curves for the four SACN05 alloys at the other two strain rates of 0.0001 $sec^{-1}$ and 0.00001 $sec^{-1}$ are shown in Figures 12-13 (water quenched) and Figures 14-15 (reflowed). Analogous trends were observed for the material property variations with temperature and alloy composition (silver content).

The effect of solidification profile on the mechanical behavior of a given SAC alloy can be shown by comparing the analogous curves from Figures 8, 12, 13 (water quenched) with those from Figures 9, 14, 15 (reflowed). For example, Figure 16 contains a comparison of the water quenched SAC305 curves in Figure 8c with the reflowed SAC305 curves from Figure 9c for the strain rate of $\dot{\varepsilon}$ = 0.001 $sec^{-1}$. The dashed WQ curves clearly indicate a much stiffer and stronger response relative to the solid RF curves due to the refined microstructures in the water quenched samples.

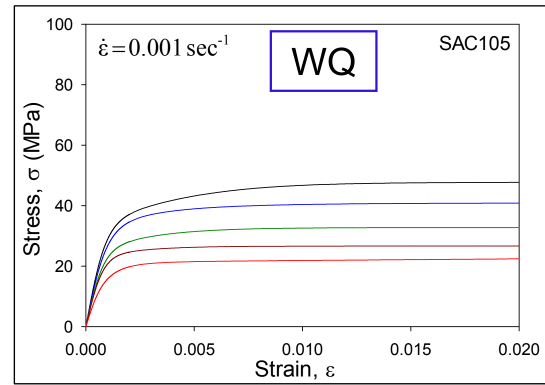


(a) SAC105

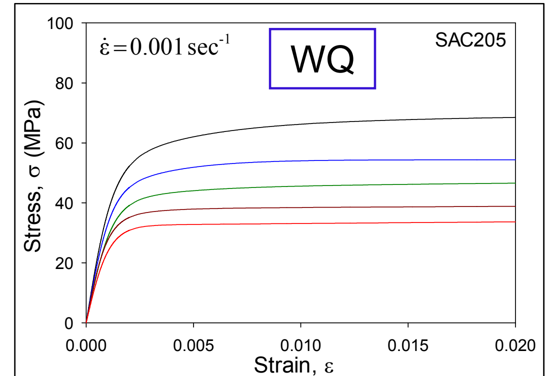


(b) SAC205

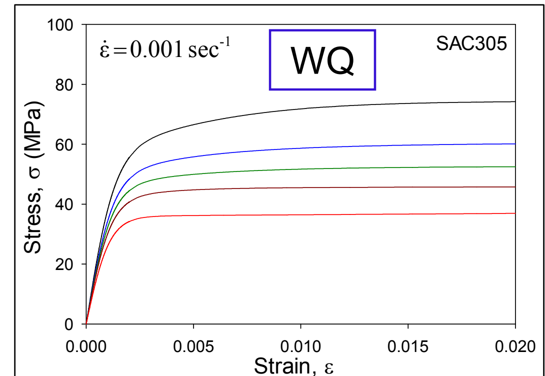


(c) SAC305

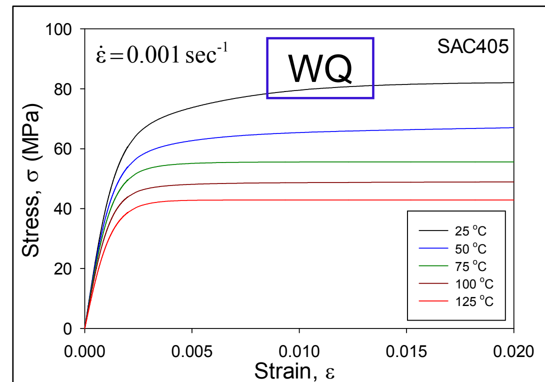


(d) SAC405

Figure 8 - Stress-Strain Curves for Strain Rate of $\dot{\varepsilon}$ = 0.001 $sec^{-1}$ [Water Quenched]

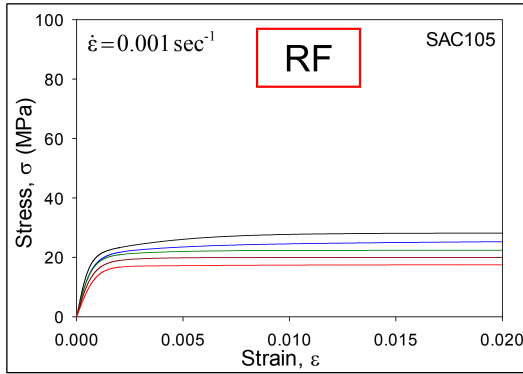


(a) SAC105

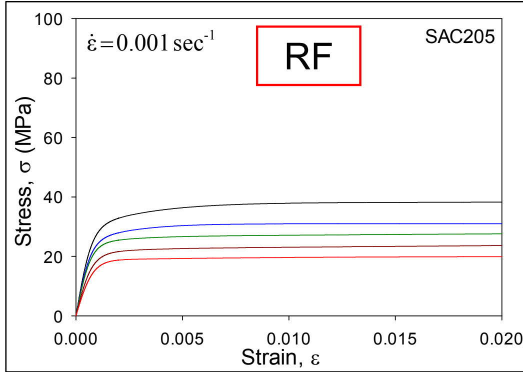


(b) SAC205

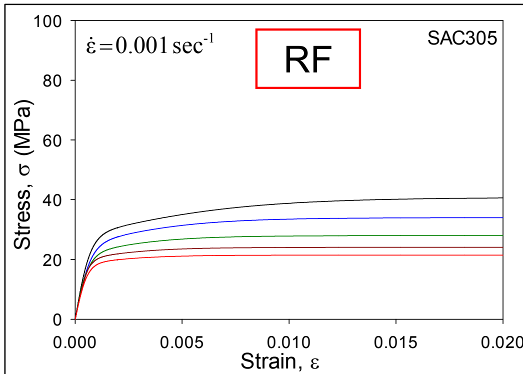


(c) SAC305

Figure 9 - Stress-Strain Curves for Strain Rate of $\dot{\varepsilon}$ = 0.001 sec$^{-1}$ [Reflowed]

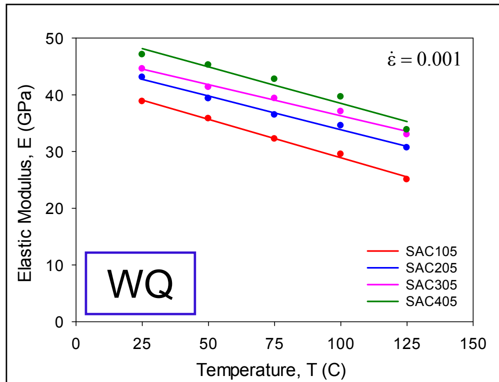


(a) Elastic Modulus

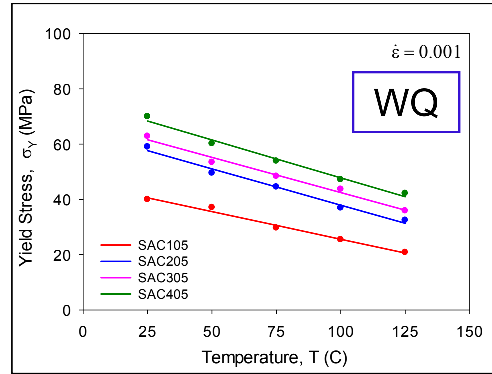


(b) Yield Strength

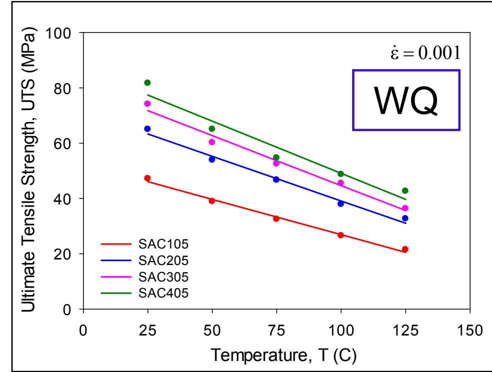


(c) Ultimate Strength

Figure 10 - Variation of Mechanical Properties with Temperature [Water Quenched]

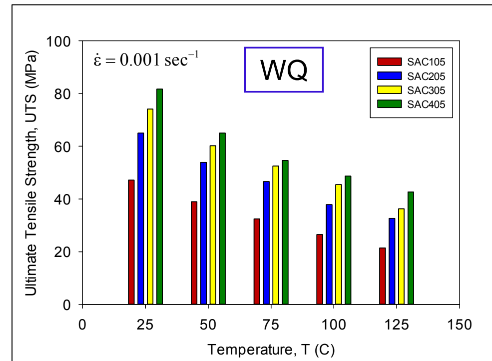


(a) Water Quenched (WQ)

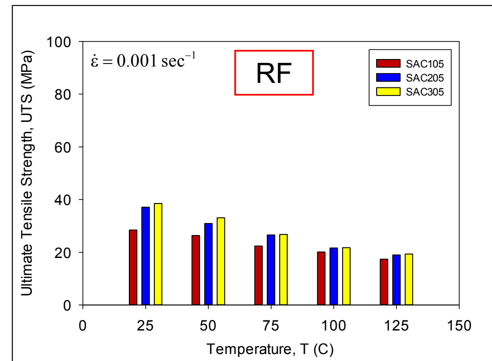


(b) Reflowed (RF)

Figure 11 - Ultimate Strength Variation for SACN05 Alloys

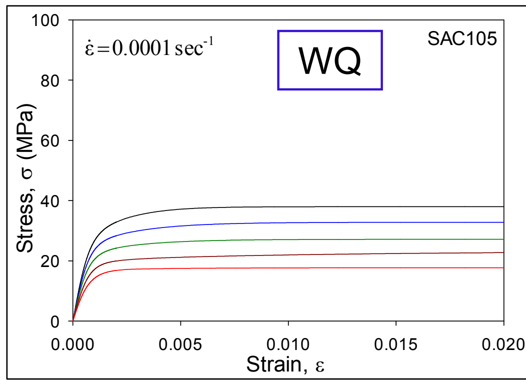


(a) SAC105

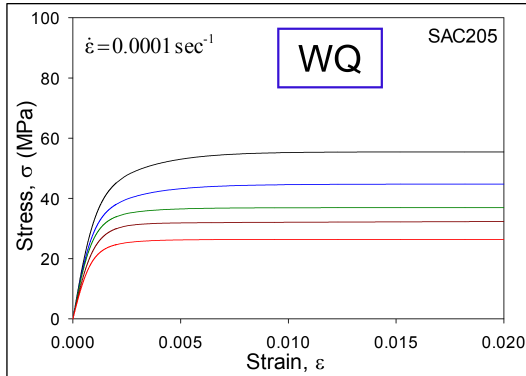


(b) SAC205

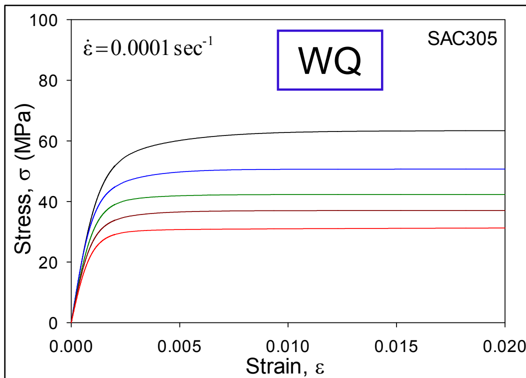


(c) SAC305

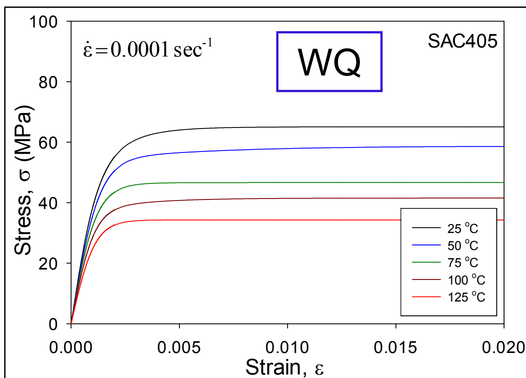


(d) SAC405

Figure 12 - Stress-Strain Curves for Strain Rate of $\dot{\varepsilon}$ = 0.0001 sec$^{-1}$ [Water Quenched]

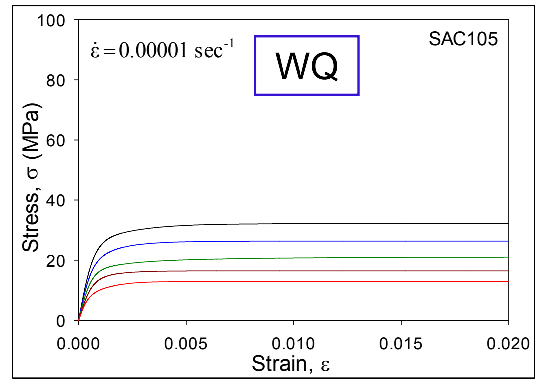


(a) SAC105

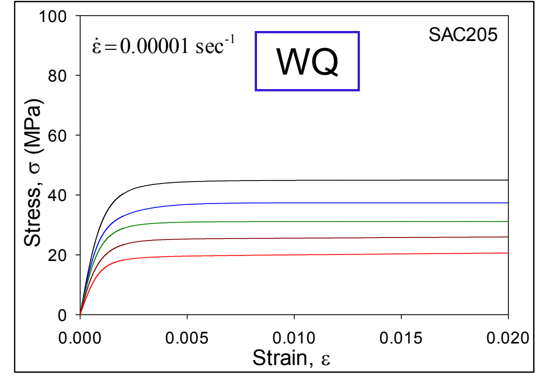


(b) SAC205

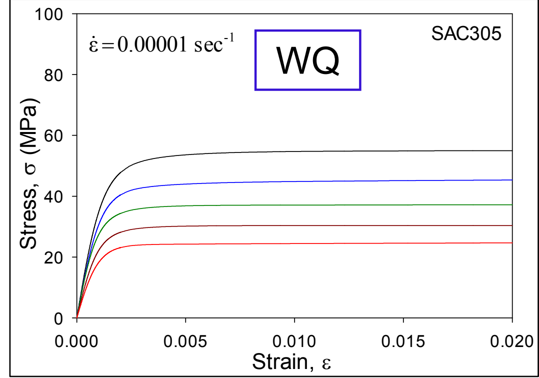


(c) SAC305

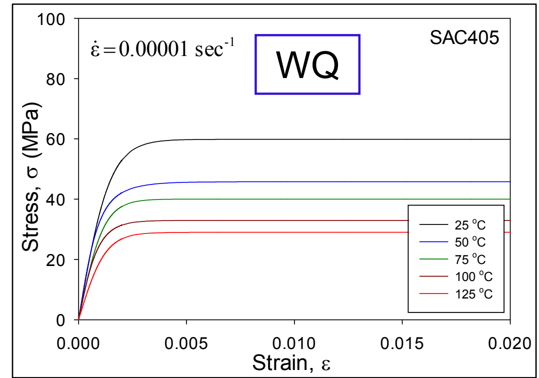


(d) SAC405

Figure 13 - Stress-Strain Curves for Strain Rate of $\dot{\varepsilon}$ = 0.00001 sec$^{-1}$ [Water Quenched]

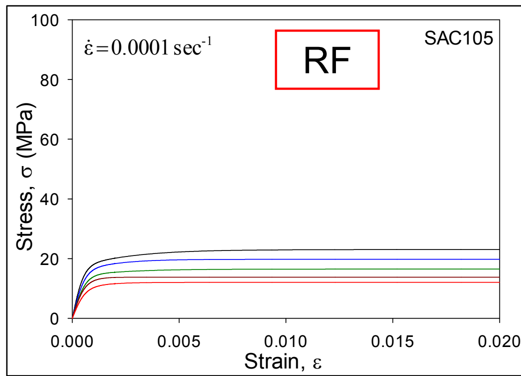

(a) SAC105

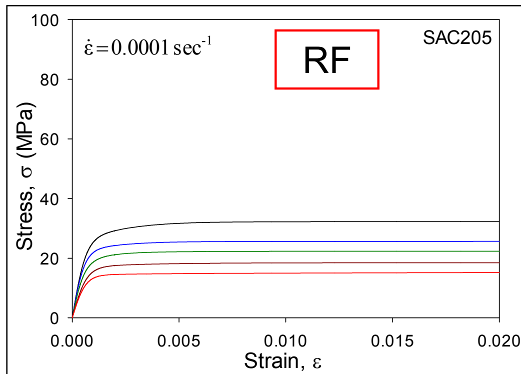

(b) SAC205

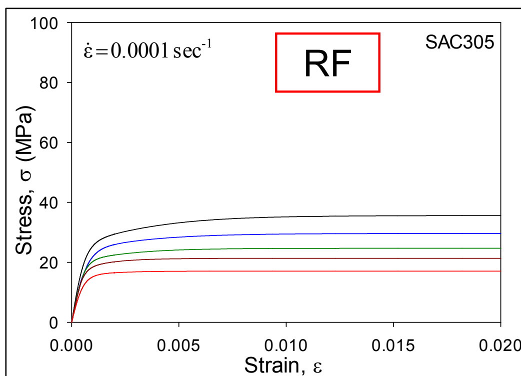

(c) SAC305

Figure 14 - Stress-Strain Curves for Strain Rate of $\dot{\varepsilon}$ = 0.0001 sec$^{-1}$ [Reflowed]

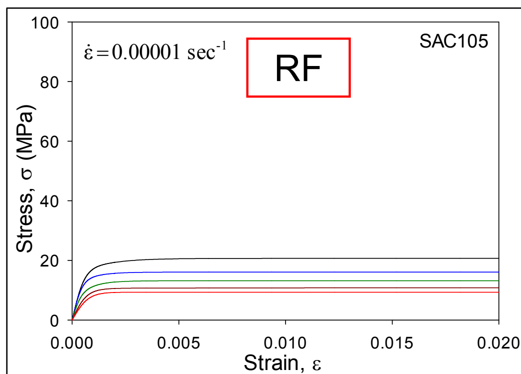

(a) SAC105

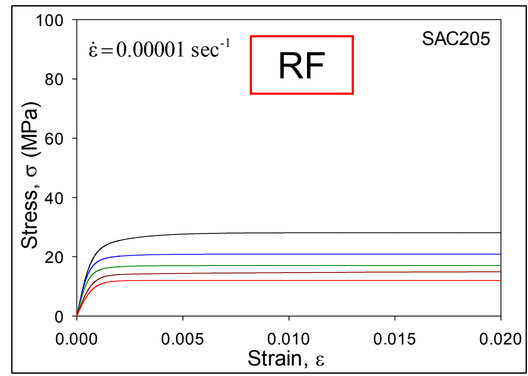

(b) SAC205

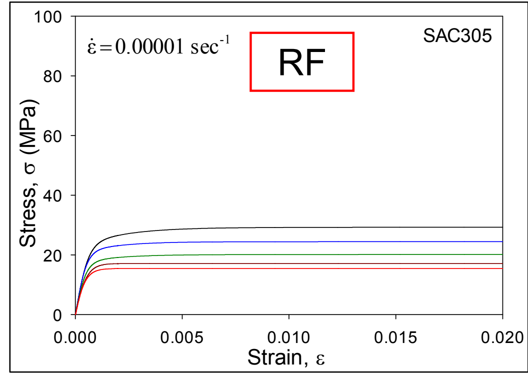

(c) SAC305

Figure 15 - Stress-Strain Curves for Strain Rate of $\dot{\varepsilon}$ = 0.00001 sec$^{-1}$ [Reflowed]

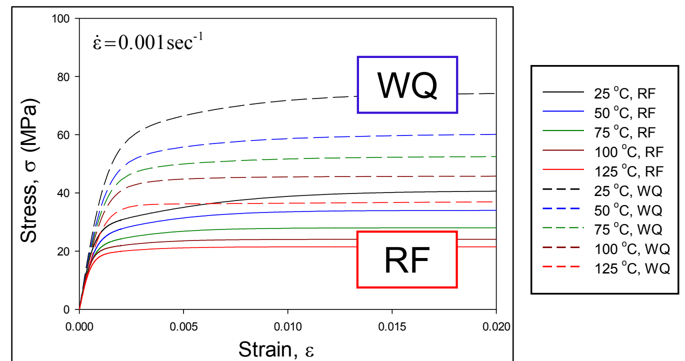


Figure 16 - Comparison of Stress-Strain Curves for SAC305 $\dot{\varepsilon}$ = 0.001 sec$^{-1}$ [WQ and RF]

Direct comparisons of the ultimate strength values for the WQ and RF SAC305 materials are shown in the bar graph in Figure 17. The UTS values of the water quenched samples are 74.1, 60.2, 52.5, 45.5, and 36.3 MPa at temperatures of 25, 50, 75, 100, and 125 C, respectively; whereas the corresponding UTS values for the reflowed samples are 38.5, 33.1, 26.8, 20.5, and 19.1 MPa. Thus, at all five temperatures, the WQ strength values are approximately twice as high as the analogous RF strength values. Similar results were observed for the yield strength (YS). However, the differences in the initial effective elastic moduli of the water quenched and

reflowed samples were smaller. The results for the other two strain rates followed the same trends.

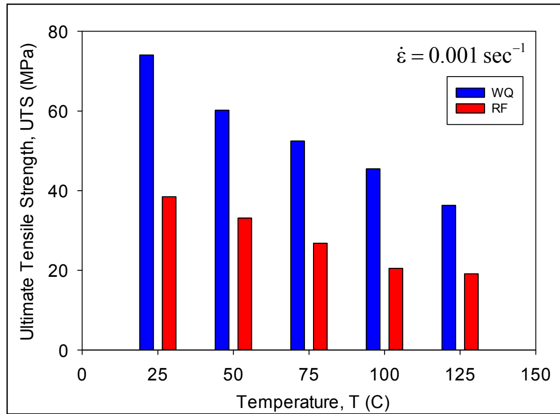


Figure 17 - Comparison of UTS Values for SAC305 $\dot{\varepsilon} = 0.001\ sec^{-1}$ [WQ and RF]

The dramatic differences in the material properties for the specimens formed using the water quenched and reflowed solidification profiles are a direct result of the microstructures present in the samples. Figure 18 illustrates the WQ and RF microstructures for the SAC305 specimens. In the water quenched samples, it can be seen in that β-Sn dendrites are very small in size and that the IMC particles are extremely fine and evenly distributed across the β-Sn matrix. For the reflowed samples with slower cooling, the β-Sn dendrites are much larger, and the IMC particles become much coarser and appear in conglomerates around the dendrites.

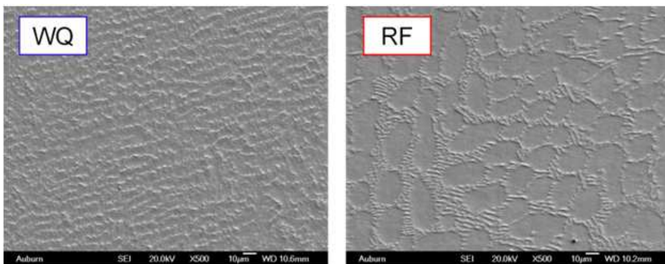


Figure 18 - Comparison of SAC305 Microstructures [WQ and RF]

**Effects of Ag Content and Solidification Profile on the Anand Model Material Parameters**

The Anand model parameters for each SACN05 (SAC105, SAC105, SAC205, SAC305 and SAC405) lead free solder material have been determined from the strain rate and temperature dependent stress-strain data shown in Figures 8-9 and 12-15. These calculations have been performed for both the water quenched and reflowed solder solidification profiles. Saturation stress (UTS) values at the various strain rates and temperatures were first extracted from the stress-strain data for each SAC alloy and solidification profile. In addition, stress vs. plastic strain data for each SAC alloy and cooling profile were found at several strain rates and temperatures. From these extracted results, the nine Anand parameters for each alloy and cooling profile were found using the using eqs. (14-15) and the nonlinear regression analysis procedure discussed above. The calculated Anand parameters for SAC105, SAC205, SAC305, and SAC405 are tabulated in Table 3 and Table 4 for water quenched and reflowed samples, respectively.

Table 3 - Anand Model Parameters for SACN05 [WQ]

| Anand Parameters | Units | SAC 105 | SAC 205 | SAC 305 | SAC 405 |
|---|---|---|---|---|---|
| $s_o$ | MPa | 16.7 | 27.9 | 32.2 | 34.35 |
| Q/R | 1/K | 8846 | 9080 | 9320 | 9560 |
| A | $sec^{-1}$ | 5500 | 3200 | 2800 | 2650 |
| ξ | Dimensionless | 4 | 4 | 4 | 4 |
| m | Dimensionless | 0.25 | 0.28 | 0.29 | 0.30 |
| $h_o$ | MPa | 142,000 | 174,000 | 186,000 | 192,000 |
| $\hat{s}$ | MPa | 38.15 | 43.00 | 44.67 | 45.51 |
| n | Dimensionless | 0.0100 | 0.0115 | 0.0120 | 0.0123 |
| a | Dimensionless | 1.85 | 1.75 | 1.72 | 1.70 |

Table 4 - Anand Model Parameters for SACN05 [RF]

| Anand Parameters | Units | SAC 105 | SAC 205 | SAC 305 | SAC 405 |
|---|---|---|---|---|---|
| $s_o$ | MPa | 7.5 | 16.5 | 21.0 | TBD |
| Q/R | 1/K | 8850 | 9090 | 9320 | TBD |
| A | $sec^{-1}$ | 6900 | 4300 | 3501 | TBD |
| ξ | Dimensionless | 4 | 4 | 4 | 4 |
| m | Dimensionless | 0.215 | 0.238 | 0.250 | TBD |
| $h_o$ | MPa | 137500 | 169000 | 180000 | TBD |
| $\hat{s}$ | MPa | 25.1 | 29 | 30.2 | TBD |
| n | Dimensionless | 0.0062 | 0.0087 | 0.0100 | TBD |
| a | Dimensionless | 1.96 | 1.84 | 1.78 | TBD |

To visualize the effects of silver content and solidification profile on the Anand model parameters for the various SACN05 alloys, the values in Table 3 and 4 have been plotted as a function of silver content (%) as shown in Figure 19. Empirical models have been used to fit the data points at integer values of the silver content, and provide estimates for the Anand parameters for other alloys with non-integer silver content percentages. In all cases, smooth monotonic variations of the parameters were found. Parameter ξ was maintained constant to keep other parameters in the same scale, and thus independent of the alloy silver content. The ratio Q/R was found to change linearly with the silver content, while the other 7 parameters ($s_o$, A, m, $h_o$, $\hat{s}$, n, and a) all exhibited nonlinear variations. For all parameters, the WQ (blue) and RF (red) variations are consistent with each other.

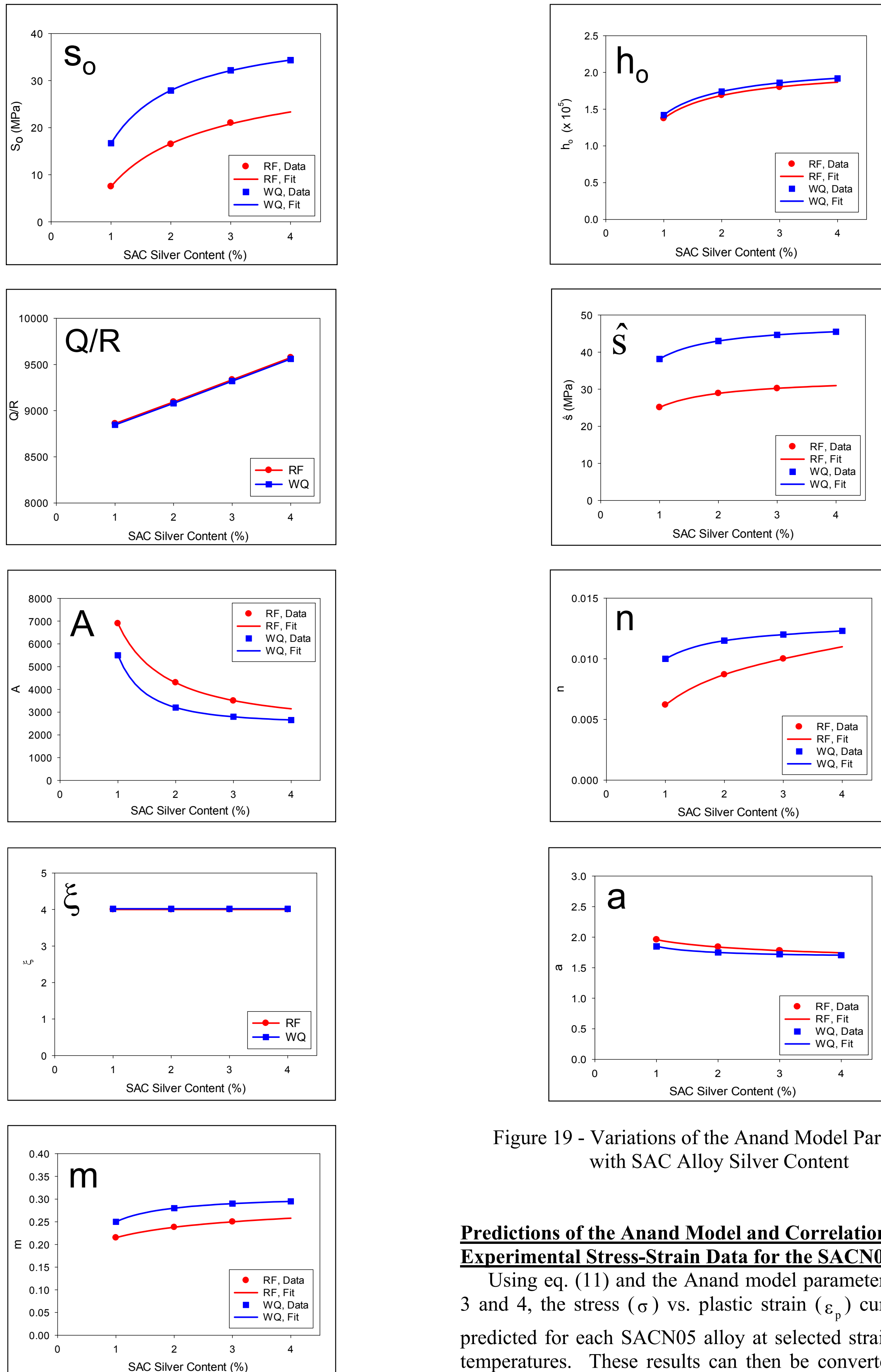


Figure 19 - Variations of the Anand Model Parameters with SAC Alloy Silver Content

**<u>Predictions of the Anand Model and Correlations with the Experimental Stress-Strain Data for the SACN05 Alloys</u>**

Using eq. (11) and the Anand model parameters in Tables 3 and 4, the stress ( $\sigma$ ) vs. plastic strain ( $\varepsilon_p$ ) curves can be predicted for each SACN05 alloy at selected strain rates and temperatures. These results can then be converted to stress ( $\sigma$ ) vs. total strain curve ( $\varepsilon$ ) by adding the elastic strain to the plastic strain:

$$\varepsilon = \varepsilon_e + \varepsilon_p \qquad \varepsilon_e = \frac{\sigma}{E} \tag{20}$$

where E is the initial elastic modulus of the SAC alloy at the selected strain rate and temperature.

Figure 20 illustrates the correlations between the Anand model stress-strain curve predictions and the experimental stress-strain data for the water quenched SACN05 alloys and a strain rate of $\dot{\varepsilon}$ = 0.001 $sec^{-1}$. In this case, the Anand model parameters tabulated in Table 3 were used with eqs. (11, 20). The experimental curves were those shown earlier in Figure 8. Excellent agreement was found between the calculated curves and the experimental data for all four of the SACN05 alloys. Analogous results for the reflowed SACN05 alloys are shown in Figure 21.

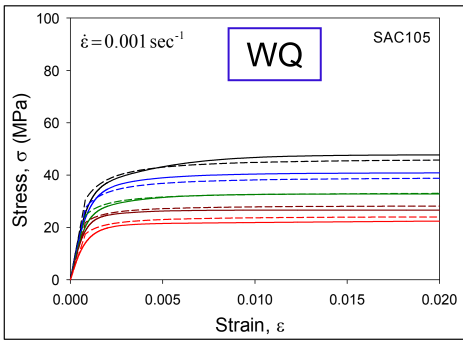

(a) SAC105

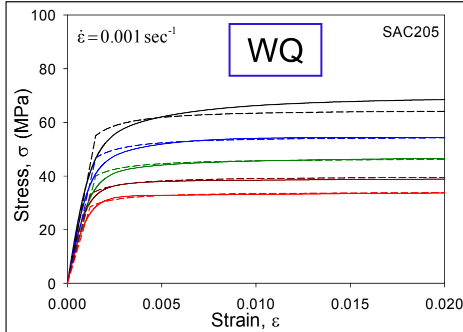

(b) SAC205

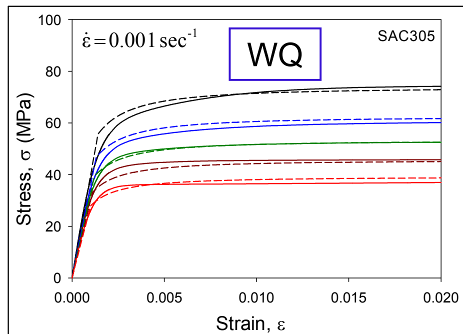

(c) SAC305

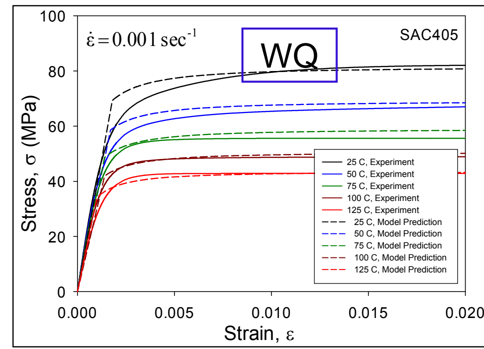

(d) SAC405

Figure 20 - Correlation of the Anand Model Predictions with Experimental Stress-Strain Data $\dot{\varepsilon}$ = 0.001 $sec^{-1}$ [Water Quenched]

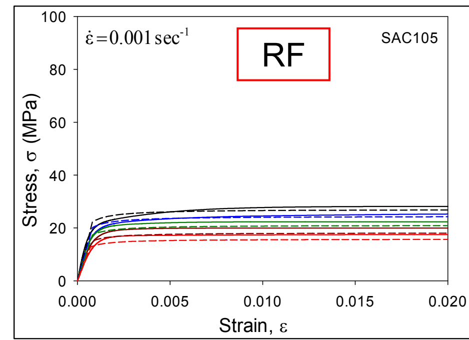

(a) SAC105

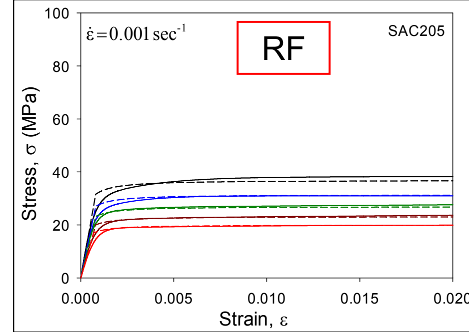

(b) SAC205

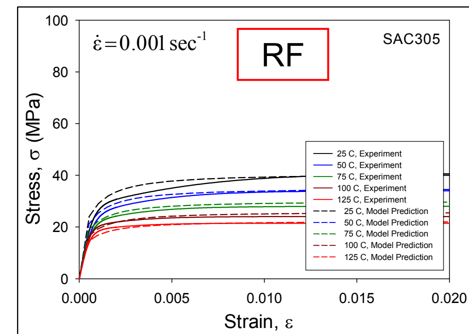

(c) SAC305

Figure 21 - Correlation of the Anand Model Predictions with Experimental Stress-Strain Data $\dot{\varepsilon}$ = 0.001 $sec^{-1}$ [Reflowed]

## SUMMARY AND CONCLUSIONS

In this work, an investigation on the Anand constitutive model and its application to SAC solders of various Ag contents (i.e. SACN05, with N = 1, 2, 3, 4) has been performed. For each alloy, both water quenched (WQ) and reflowed (RF) solidification profiles were utilized to establish two unique specimen microstructures, and the same reflow profile was used for all four of the SAC alloys so that the results could be compared and the effects of Ag content could be studied systematically.

The nine Anand parameters were determined for each unique solder alloy and microstructure from a set of stress-strain tests performed at several strain rates and temperatures. Testing conditions included strain rates of $\dot{\varepsilon} = 0.001, 0.0001$, and 0.00001 ($sec^{-1}$), and temperatures of T = 25, 50, 75, 100, and 125 C. The Anand parameters were calculated from each set of stress-strain data using a two-step nonlinear regression procedure. Using the calculated results for the various SAC alloys and microstructures, a set of empirical fitting curves have been established to describe the effects of SAC alloy Ag content on the Anand model parameters.

As expected, the mechanical properties (modulus and strength) increase with the percentage of Ag content, and these changes strongly affect the Anand parameters. The sensitivity of the mechanical properties and Anand parameters to silver content is higher at lower silver contents (1-2%). Also, the observed mechanical properties of water quenched samples were better (higher in magnitude) than the corresponding mechanical properties of the reflowed samples. Although the differences in elastic modulus between the water quenched and reflowed samples are small, significant differences are present for the yield and ultimate tensile stresses of all four SAC alloys. After deriving the Anand parameters for each alloy, the stress-strain curves have been calculated for various conditions, and excellent agreement was found between the predicted results and experimental stress-strain curves.

## ACKNOWLEDGMENTS

This work was supported by the NSF Center for Advanced Vehicle and Extreme Environment Electronics ($CAVE^3$).

## REFERENCES


1. Zeng, K., and Tu, K. N., "Six Cases of Reliability Study of Pb-Free Solder Joints in Electronic Packaging Technology," *Materials Science and Engineering R*, Vol 38(2), pp. 55-105, 2002.
2. Terashima, S., Kariya, Y., Hosoi, T., and Tanaka, M., J., "Effect of Silver Content on Thermal Fatigue Life of Sn-Xag-0.5Cu Flip-Chip Interconnects," *Journal of Electronic Materials*, Vol. 32(12), pp. 1527-1533, 2003.
3. Amagai, M., Toyoda, Y., and Tajima, T., "High Solder Joint Reliability with Lead Free Solders," *Proceedings of Electronic Components and Technology Conference*, pp. 317-322, 2003.
4. Ma, H., and Suhling, J. C., "A Review of Mechanical Properties of Lead-Free Solders for Electronic Packaging," *Journal of Materials Science*, Vol. 44, pp. 1141-1158, 2009.
5. Che, F. X., Zhu, W. H., Pow, E. S. W., Zhang, X. W., and Zhang, X. R., "The Study of Mechanical Properties of Sn-Ag-Cu Lead-Free Solders with Different Ag Contents and Ni Doping Under Different Strain Rates and Temperatures," *Journal of Alloys and Compounds,* Vol. 507(1), pp. 215-224, 2010.
6. Zhu, F., Zhang, H., Guan, R., and Liu, S., "Effects of Temperature and Strain Rate on Mechanical Property of Sn96.5Ag3Cu0.5," *Journal of Alloys and Compounds,* Vol. 438(1), pp.100-105, 2007.
7. Ma, H., Suhling, J. C., Lall P., Bozack, M. J., "Reliability of the Aging Lead-free Solder Joint," *Proceeding of the 56th Electronic Components and Technology Conference*, San Diego, CA, pp. 849-864, 2006
8. Ma, H., Suhling, J. C., Zhang, Y., Lall, P., and Bozack, M. J., "The Influence of Elevated Temperature Aging on Reliability of Lead Free Solder Joints," *Proceedings of the 57th IEEE Electronic Components and Technology Conference*, pp. 653-668, Reno, NV, May 29-June 1, 2007.
9. Zhang, Y., Cai, Z., Suhling, J. C., Lall, P., and Bozack, M. J., "The Effects of Aging Temperature on SAC Solder Joint Material Behavior and Reliability," *Proceedings of the 58th IEEE Electronic Components and Technology Conference*, pp. 99-112, Orlando, FL, May 27-30, 2008.
10. Zhang, Y., Cai, Z., Suhling, J. C., Lall, P., and Bozack, M. J., "The Effects of SAC Alloy Composition on Aging Resistance and Reliability," *Proceedings of the 59th IEEE Electronic Components and Technology Conference*, pp. 370-389, San Diego, CA, May 27-29, 2009.
11. Zhang, Y., Kurumaddali, K., Suhling, J. C., Lall, P., and Bozack, M. J., "Analysis of the Mechanical Behavior, Microstructure, and Reliability of Mixed Formulation Solder Joints," *Proceedings of the 59th IEEE Electronic Components and Technology Conference*, pp. 759-770, San Diego, CA, May 27-29, 2009.
12. Cai, Z., Zhang, Y., Suhling, J. C., Lall, P., Johnson, R. W., Bozack, M. J., "Reduction of Lead Free Solder Aging Effects using Doped SAC Alloys," *Proceedings of the 60th Electronic Components and Technology Conference*, pp. 1493-1511, 2010.
13. Mustafa M., Cai Z., Suhling J. C., Lall P., "The Effects of Aging on the Cyclic Stress-Strain Behavior and Hysteresis Loop Evolution of Lead Free Solders," *Proceedings of the 61st Electronic Components and Technology Conference*, pp. 927-939, 2011.
14. Mustafa, M., Cai, Z., Roberts, J. R., Suhling, J. C., Lall, P., "Evolution of the Tension/Compression and Shear Cyclic Stress-Strain Behavior of Lead-Free Solder Subjected to Isothermal Aging," *Proceedings of ITherm 2012*, pp. 765-780, San Diego, CA, May 30 - June 1, 2012.
15. Zhang, J., Hai, Z., Thirugnanasambandam, S., Evans, J. L., Bozack, M. J., Sesek, R., Zhang, Y., Suhling, J. C., "Correlation of Aging Effects on Creep Rate and Reliability in Lead Free Solder Joints," *SMTA Journal*, Volume 25(3), pp. 19-28, 2012.

16. Zhang, J., Hai, Z., Thirugnanasambandam, S., Evans, J. L., Bozack, M. J., Zhang, Y., Suhling, J. C., "Thermal Aging Effects on Thermal Cycling Reliability of Lead-Free Fine Pitch Packages," *IEEE Transactions on Components and Packaging Technologies*, Vol. 3(8), pp. 1348-1357, 2013.
17. Motalab, M., Cai, Z., Suhling, J. C., Zhang, J., Evans, J. L., Bozack, M. J., Lall, P., "Improved Predictions of Lead Free Solder Joint Reliability that Include Aging Effects," *Proceedings of the 62nd IEEE Electronic Components and Technology Conference*, pp. 513-531, San Diego, CA, May 30 - June 1, 2012.
18. Motalab, M., Cai, Z., Suhling, J. C., Zhang, J., Evans, J. L., Bozack, M. J., Lall, P., "Correlation of Reliability Models Including Aging Effects with Thermal Cycling Reliability Data," *Proceedings of the 63rd IEEE Electronic Components and Technology Conference*, pp. 986-1004, Las Vegas, NV, May 28-31, 2013.
19. Hasnine, M., Mustafa, M., Suhling, J. C., Prorok, B. C., Bozack, M. J., Lall, P., "Characterization of Aging Effects in Lead Free Solder Joints Using Nanoindentation," *Proceedings of the 63rd IEEE Electronic Components and Technology Conference*, pp. 166-178, Las Vegas, NV, May 28-31, 2013.
20. Lall, P., Shantaram, S., Suhling, J., Locker, D., "Effect of Aging on the High Strain Rate Mechanical Properties of SAC105 and SAC305 Leadfree Alloys," *Proceedings of the 63rd IEEE Electronic Components and Technology Conference*, pp. 1277-1293, Las Vegas, NV, May 28-31, 2013.
21. Anand, L., "Constitutive Equations for the Rate-Dependent Deformation of Metals at Elevated Temperatures," *Journal of Engineering Materials and Technology*, Vol. 104(1), pp. 12-17, 1982.
22. Amagai, M., Watanabe, M., Omiya, M., Kishimoto, K., and Shibuya, T., "Mechanical Characterization of Sn-Ag Based Lead-Free Solders," *Microelectronics Reliability*, Vol. 42(6), pp. 951-966, 2002.
23. Herkommer, D., Punch, J. and Reid, M., "A Reliability Model for SAC Solder Covering Isothermal Mechanical Cycling and Thermal Cycling Conditions," *Microelectronics Reliability,* Vol. 50, pp. 116-126, 2010.
24. Wang, G. Z., Cheng, Z. N., Becker, K., Wilde, J., "Applying Anand Model to Represent the Viscoplastic Deformation Behavior of Solder Alloys," *Journal of Electronic Packaging*, Vol. 123(3), pp. 247-253, 2001.
25. Bhate, D., Chan, D., Subbarayan, G., Chiu, T., Gupta, V., and Edwards, D., "Constitutive Behavior of Sn3.8Ag0. 7Cu and Sn1.0Ag0.5Cu Alloys at Creep and Low Strain Rate Regimes," *IEEE Transactions on Components and Packaging Technology,* Vol. 31(3), pp. 622–633, 2008.
26. Che, F., Pang, H., Zhu, W., Sun, W., and Sun, A., "Modeling Constitutive Model Effect on Reliability of Lead-Free Solder Joints," *Proceedings of the 7th International Conference on Electronics Packaging Technology,* pp. 1-6, 2006.
27. Pei, M., and Qu, J., "Constitutive Modeling of Lead-Free Solders," *Proceedings of the International Symposium on Advanced Packaging Materials,* pp. 45-49, 2005.
28. Mysore, K., Subbarayan, G., Gupta, V., and Zhang, R., "Constitutive and Aging Behavior of Sn3.0Ag0.5Cu Solder Alloy," *IEEE Transactions, Electronics Packaging and Manufacturing*, Vol. 32(4), pp. 221-232, 2009.
29. Motalab, M. A., Cai, Z. Suhling, J. C., Lall, P., "Determination of Anand Constants for SAC Solders Using Stress-Strain or Creep Data," *Proceedings of ITherm 2012*, pp. 910-922, 2012.
30. Bai, N., Chen, X., and Gao, H., "Simulation of Uniaxial Tensile Properties for Lead-Free Solders with Modified Anand Model," *Materials and Design,* Vol. 30, pp. 122-128, 2009.
31. Kim, Y., Noguchi, H., and Amagai, M., "Vibration Fatigue Reliability of BGA-IC Package With Pb-Free Solder and Pb-Sn Solder," *Proceedings of 53rd Electronic Components and Technology Conference,* pp. 891-897, 2003.
32. Li, D., Liu, C., and Conway, P. P., "Microstructure and Shear Strength Evolution of Sn-Ag-Cu Solder Bumps During Aging at Different Temperatures," *Journal of Electronic Materials*, Vol. (35), pp. 388-398, 2006.